Journal of Nuclear Materials 407 (2010) 220–227

Contents lists available at ScienceDirect

Journal of Nuclear Materials

journal homepage: www.elsevier.com/locate/jnucmat

Computational study of atomic mobility for the bcc phase of the U–Pu–Zr ternary system

Weibang Li [a], Rui Hu [a,*], Y.-W. Cui [b,c], Hong Zhong [a], Hui Chang [a], Jinshan Li [a], Lian Zhou [a]

[a] State Key Laboratory of Solidification Processing, Northwestern Polytechnical University, Xi'an 710072, PR China
[b] Department of Materials Science and Engineering, Ohio State University, Columbus, OH 43210, USA
[c] Madrid Institute for Advanced Studies in Materials, IMDEA Materials, C/Profesor Aranguren s/n, 28040 Madrid, Spain

ARTICLE INFO

Article history:
Received 21 June 2010
Accepted 22 October 2010

ABSTRACT

Experimental diffusion data in literature has been evaluated to assess the atomic mobility for the bcc phase in the U–Pu–Zr system by means of the DICTRA-type (Diffusion Controlled TRAnsformation) phenomenological treatment. The developed mobility database has been validated by comprehensive comparisons made between the experimental and calculated diffusion coefficients, as well as other interesting details resulting from interdiffusion, e.g. the concentration profile and the diffusion path of diffusion couples.

1. Introduction

The U–Pu–Zr alloy has been widely used as a fuel material due to its unique combination of high solidus temperature and improved characteristics (e.g. high burn-up capability, favorable thermal response) in fuel/cladding chemical interactions during steady-state reactor operation, as well as its inherent safety characteristics [1]. It is well known that constituent redistribution, therefore microstructure and property, in metallic fuels inevitably occurs due to the solid-state diffusion under thermal and chemical driving forces that might be further enhanced by irradiation. The knowledge of thermodynamics and diffusion is of crucial importance to understanding and predicting the microstructural development and evolution of nuclear fuel during its life cycle [2]. The study of thermo-kinetic properties is also driven by increasing demands for computer simulation of microstructural evolution, with the phase field approach as one representative, developing toward a quantitative model.

However, reliable diffusion experiments at high temperatures are hard to perform; this is particularly true for the U–Pu–Zr ternary alloys due to their affinity for oxygen and radioactive nature. An efficient way to study the diffusion is the DICTRA-type (Diffusion Controlled TRAnsformation) phenomenological treatment, in which the atomic mobility, rather than diffusivity, is used as a base [3,4]. This treatment makes the DICTRA-type diffusion modeling practical for creating kinetic databases and performing diffusion modeling, even for commercially important multicomponent systems, because it defines one unique mobility for each component in a multicomponent system. More importantly, the mobility database can be used in conjunction with the CALPHAD-base (Calculation of Phase Diagram) thermodynamics database to obtain sufficiently reliable thermodynamic quantities, thus having the ability to offer a full diffusion picture of alloys of interest without extra experimental measurements. It should be noted that some important assumptions and/or simplifications have been made in the DICTRA-type mobility formalism, for example, (i) the Darken relation is used, i.e. no vacancy wind or any other correction term is considered; (ii) off-diagonal *mobility* terms are ignored (i.e. correlation effects are assumed to be negligible); (iii) all the species have the same partial molar volumes, and (iv) the composition dependence of the mobility is assumed to follow the Redlich–Kister expansion.

So far, there is a thermodynamics database [1,5] and some experimental diffusion data [6,7] available for the U–Pu–Zr system, however, no atomic mobility database is available yet. Therefore, the objectives of the present study are to evaluate the diffusion data to assess the atomic mobility for the bcc phase of the U–Pu–Zr ternary, and then use the validated atomic mobility database to predict a full diffusion picture for the bcc U–Pu–Zr ternary alloys.

2. Modeling description

2.1. Atomic mobility and diffusivity

Andersson and Ågren [4] suggested that the atomic mobility M_i of species i could be expressed as a function of temperature T,

$$M_i = M_i^0 \exp\left(\frac{-Q_i^S}{RT}\right)\frac{1}{RT}{}^{mg}\Gamma \tag{1}$$

* Corresponding author.
E-mail address: lijsh2009@gmail.com (R. Hu).

0022-3115/$ - see front matter © 2010 Elsevier B.V. All rights reserved.
doi:10.1016/j.jnucmat.2010.10.035

Table 1
Experimental diffusion data selected in the present optimization for the U–Zr system.

Diffusion data type	Method	Temperature (K)	Composition range	Year	Reference
D_U^U	LS	1073–1323	100 at.% U	1959	[10]
D_U^U	TST	1053–1353	100 at.% U	1964	[11]
D_{Zr}^{Zr}	SS	1200–1520	100 at.% Zr	1992	[12]
D_{Zr}^{Zr}	SS	1174–2020	100 at.% Zr	1964	[13]
D_U^*, D_{Zr}^*	LS	1073–1338	100 at.% U	1968	[14]
D_U^*	LS	1173–1873	100 at.% Zr	1971	[15]
$\tilde{D}_U^{Zr}$	DC	973–1223	10–95 at.% Zr	1996	[16]
$\tilde{D}_U^{Zr}$	DC	1223–1723	15 at.% U	1967	[17]
$\tilde{D}_U^{Zr}$	DC	1223–1348	10–95 at.% Zr	1956	[18]
$\tilde{D}_U^{Zr}$	DC	1223–1358	100 at.% U	1997	[19]
$\tilde{D}_U^{Zr}$	DC	973–1023	68–78 at.% Zr	1998	[20]

LS denotes lathe sectioning technique, TST denotes the thin-layer sectioning technique, SS denotes the serial sectioning technique, DC denotes the diffusion couple.

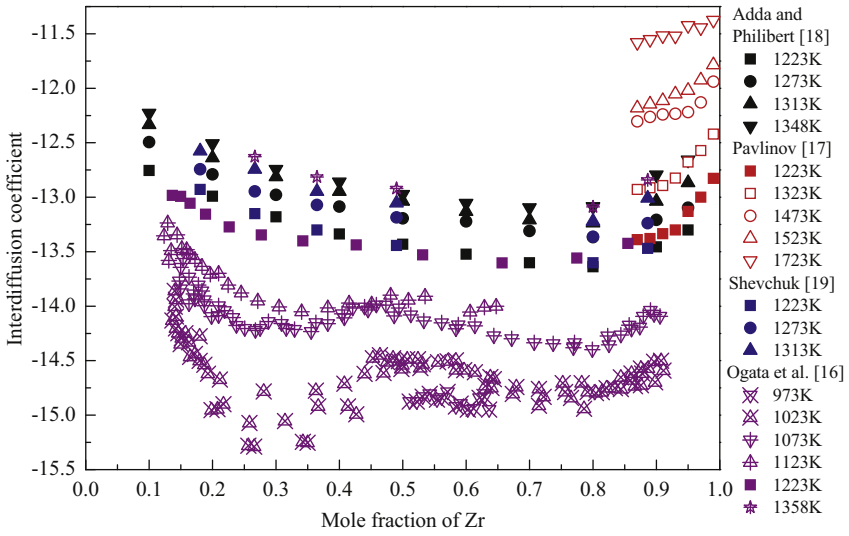

Fig. 1. Experimental information on the interdiffusion coefficients in the U–Zr system.

where M_i^0 is the frequency factor, Q_i^S is the activation energy, R is the gas constant and ${}^{mg}\Gamma$ is a factor to account for the effect of ferromagnetic ordering. In cases when the magnetic ordering is negligible, like the U–Pu–Zr ternary system, the frequency and activation terms can be grouped into a single parameter, $Q_i = -Q_i^S + RT\ln M_i^0$. Similar to the phenomenological CALPHAD approach, the parameter Q_i is approximated to be compositionally dependent [8] and this can be expressed by a Redlich–Kister polynomial [9],

$$Q_i = \sum_p x_p Q_i^p + \sum_p \sum_{q>p} x_p x_q \left[\sum_{r=0,1,2,\cdots}^{r} Q_i^{p,q} (x_p - x_q)^r \right] + \sum_p \sum_{q>p} \sum_{v>q} x_p x_q x_v \left[v_{pqv}^S {}^S Q_i^{p,q,v} \right], (S = p, q, v) \quad (2)$$

where x_p is the mole fraction of species p, Q_i^p is the value Q_i of species i in pure species p, ${}^r Q_i^{p,q}$ and ${}^S Q_i^{p,q,v}$ are the binary and ternary interaction parameters. Various diffusivities can be directly related to the atomic mobility, e.g., the tracer diffusion coefficient D_i^* is rigorously related to the atomic mobility, M_i, by a simple relation:

$$D_i^* = RTM_i, \quad (3)$$

the intrinsic diffusion coefficient, e.g., for a binary alloy with a constant molar volume, by:

$$D_i = x_i M_i \left(\frac{\partial \mu_i}{\partial x_i} - \frac{\partial \mu_i}{\partial x_j} \right), (j \neq i), \quad (4)$$

where μ_i is the chemical potential of species i, and the interdiffusion coefficients, $\tilde{D}_{pq}^n$, relative to dependent species n, is derived by a form [8]

$$\tilde{D}_{pq}^n = \sum_{i=1}^{n-1} (\delta_{ip} - x_p) x_i M_i \left(\frac{\partial \mu_i}{\partial x_q} - \frac{\partial \mu_i}{\partial x_n} \right), \quad (5)$$

where the Kronecker delta $\delta_{ip} = 1$ when $i = p$ and 0 otherwise. Upon the proposed relations, the atomic mobility parameters in Eq. (2), such as Q_i^p, ${}^r Q_i^{p,q}$ and ${}^S Q_i^{p,q,v}$, can be numerically assessed by fitting to the experimental diffusion coefficients.

The composition, varying with the diffusion time t in the diffusion zone of diffusion couple, can be described by the equation of continuity:

$$\frac{1}{V_m} \frac{\partial x_i}{\partial t} + \nabla \cdot \tilde{J}_i = 0, \quad (6)$$

where V_m is the molar volume which is generally treated as constant, and $\tilde{J}_i$ is the interdiffusion flux of component i. With different initial conditions and boundary conditions, Eq. (6) can be solved numerically to express the form of the concentration profile. If the diffusion process is controlled by a vacancy mechanism, the non-uniform velocity of the inert markers, measured in the laboratory-fixed frame of reference, can be derived from the difference of the intrinsic diffusion flux J_i:

$$v = -V_m(J_A + J_B) = (D_B - D_A)\frac{\partial x_B}{\partial z}. \quad (7)$$

3. Evaluation of experimental data

There is some experimental diffusion data available for the U–Pu–Zr bcc alloys, including tracer, impurity, and interdiffusion coefficients [6,7,10–28]. In the subsections that follow, the data is evaluated system by system.

3.1. The U–Zr binary

The experimental diffusion data for the bcc U–Zr alloys [10–20] are summarized in Table 1. The self-diffusivity of bcc-U was determined by Adda and Kirianenko [10] by using the lathe sectioning technique and by Bochvar et al. [11] by a thin-layer sectioning technique. Both works revealed that the Arrhenius relation holds for the self-diffusion in bcc-U. The studies for the self-diffusion of bcc-Zr, by Patil [12] at 1200–1520 K and by Lundy et al. [13] at 1174–2020 K, showed that the Arrhenius plot of the bcc-Zr self-diffusion is anomalously curved. Fedorov et al. [14] studied the impurity diffusivity of ^{95}Zr in bcc-U and ^{235}U in bcc-Zr from 1073 to 1338 K, both of which were shown to follow a rigorous Arrehenius relation. Afterward, however, the same research group [15] reported the latter as a curved Arrehenius plot.

The interdiffusion of the bcc U–Zr system was studied by Ogata et al. [16] in the temperature range from 973 to 1223 K by using the diffusion couple technique. A remarkable drop of the interdiffusion coefficients was detected at 1023 and 1073 K due to the demixing of the species in (or close to) the miscibility gap. Among other studies on the U–Zr system include those by Pavlinov [17] at 1223–1723 K, by Adda and Philibert [18] at 1223–1348 K, by Shevchuk [19] in a composition range of 10–90 at.% Zr at 1223–1358 K, and by Akabori [20] with 68–78 at.% Zr at 923–1023 K, respectively. As shown in Fig. 1, the data by Pavlinov [17], Adda and Philibert [18] and Shevchuk [19] agree favorably over the entire temperature range, and therefore were given the highest weight during the optimizing process. Ogata et al. [16] detected the existence of the miscibility gap, however, the derived diffusion rate was given relatively low weight because it lacked collaboration

Table 2
Assessed atomic mobilities for the bcc phase of the U–Pu–Zr ternary system (all in SI units).

Mobility	Parameter (J/mol)	Reference
Mobility of Pu		
Q_{Pu}^{Pu}	−73586.5 − 113.1*T	Present work
Q_{Pu}^{U}	48194.3248 − 279.9*T	Present work
Q_{Pu}^{Zr}	R*T*Ln[1.68E − 3*exp(−223591/R/T) + 6.55E − 15*exp(−12121.2/R/T)]	Present work
${}^0Q_{Pu}^{Pu,U}$	31175.7	Present work
${}^0Q_{Pu}^{Pu,Zr}$	−41195.1	Present work
${}^0Q_{Pu}^{U,Zr}$	−22089.8	Present work
Mobility of U		
Q_{U}^{U}	−107943.2 − 135.2*T	Present work
Q_{U}^{Pu}	−367565.657 + 104.1*T	Present work
Q_{U}^{Zr}	R*T*Ln[3.6E − 5*exp(−242400/R/T) + 5.3E−10*exp(−82300/R/T)]	[15]
${}^0Q_{U}^{Pu,U}$	−2399724.2	Present work
${}^0Q_{U}^{U,Zr}$	−23537.87 − 54.27*T	Present work
${}^1Q_{U}^{U,Zr}$	312070.48 − 176.99*T	Present work
${}^2Q_{U}^{U,Zr}$	−252306.31 + 187.94*T	Present work
${}^3Q_{U}^{U,Zr}$	6979.57	Present work
Mobility of Zr		
Q_{Zr}^{Pu}	−37784.7 − 175.7*T	Present work
Q_{Zr}^{U}	−68383.1 − 206.3*T	Present work
Q_{Zr}^{Zr}	R*T*Ln[3.2E − 7*exp(−167746/T/R) + 1.14E − 10*exp(−73741/R/T)]	Present work
${}^0Q_{Zr}^{Pu,U}$	171261.285	Present work
${}^0Q_{Zr}^{Pu,Zr}$	−4368.7	Present work
${}^0Q_{Zr}^{U,Zr}$	−277639.59 + 166*T	Present work
${}^1Q_{Zr}^{U,Zr}$	−81672.40 + 23.04*T	Present work
${}^2Q_{Zr}^{U,Zr}$	−42148.42 + 36.49*T	Present work
${}^3Q_{Zr}^{U,Zr}$	735973.01	Present work

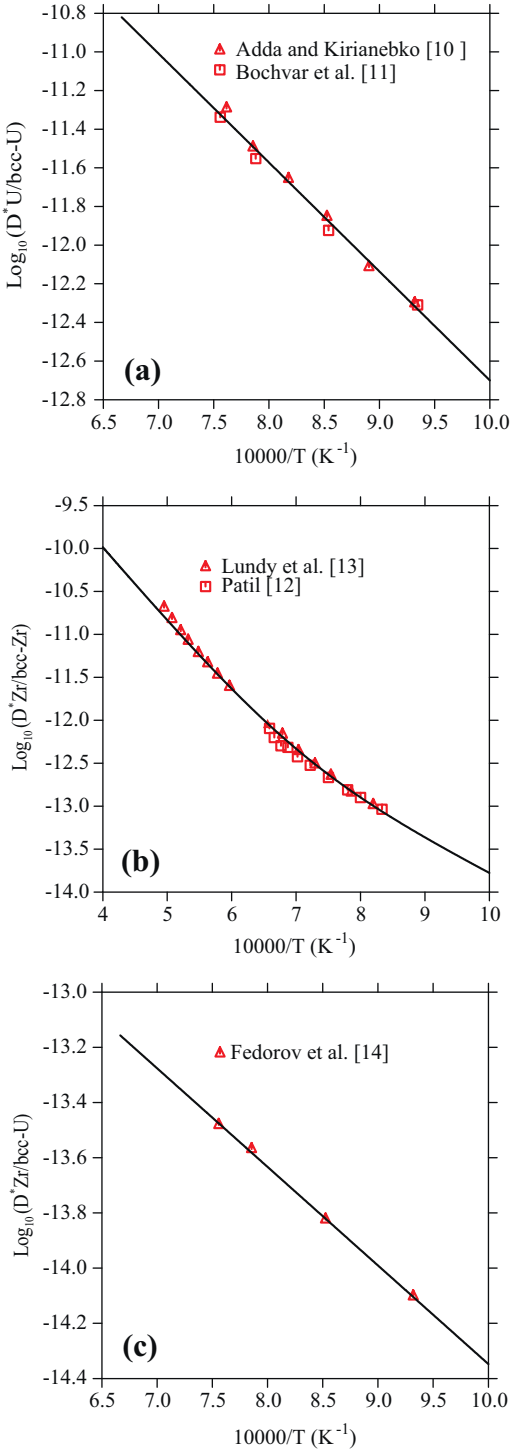

Fig. 2. Arrhenius plots of (a) the self-diffusion of bcc-U; (b) the self-diffusion of bcc-Zr and (c) the tracer diffusion of Zr in bcc-U. Symbols are the experimental points [10–14].

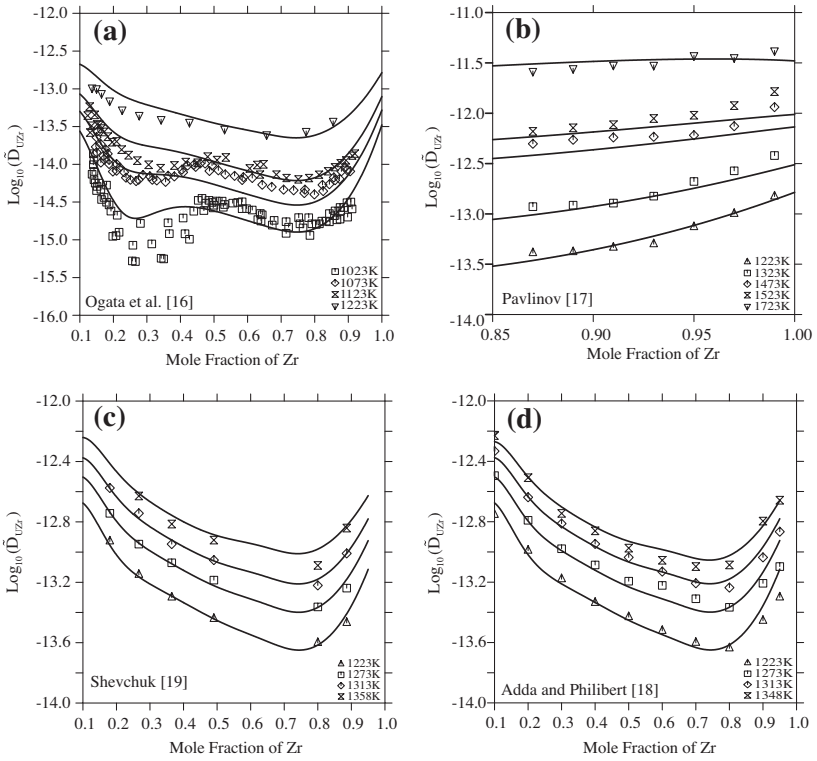

Fig. 3. Calculated interdiffusion coefficients of the bcc U–Zr alloys. Symbols are the experimental measurement from (a) Ogata et al. [16]; (b) Pavlinov [17]; (c) Shevchuk [19] and (d) Adda and Philibert [18].

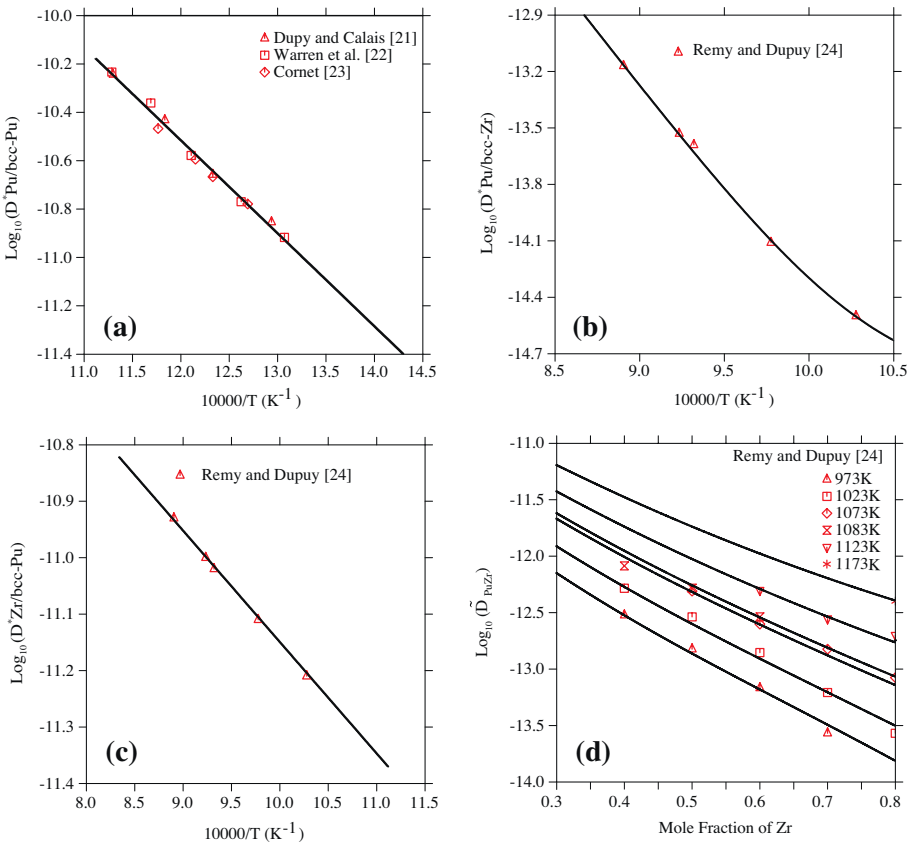

Fig. 4. Arrhenius plots of (a) the Pu self-diffusion; (b) the Pu impurity diffusion in bcc-Zr; (c) the Zr impurity diffusion in bcc-Pu and (d) interdiffusion coefficients in the bcc Pu–Zr binary system. Symbols are from the experimental measurements [21–24].

from the others and its poor purity of starting materials. The data from Akabori et al. [20] exhibits some scattering, and was excluded from the optimization.

3.2. The Pu–Zr binary

The self-diffusivity of bcc-Pu was determined to obey a linear Arrhenius relation [21–23]. The interdiffusion in the (ε-Pu, β-Zr) bcc solid solution was studied by Remy et al. [24] at the temperatures 973–1173 K, in which the Kirkendall plane was observed to shift toward the Pu-rich side.

3.3. The U–Pu–Zr ternary

Alekseev et al. [6] and Shmakov and Smirnov [7] reported a theoretical study of the interdiffusion behavior for the bcc alloys at the U-rich corner at 1073 and 1173 K, respectively. The calculations showed that both main and cross interdiffusion coefficients exhibit a strong concentration dependence and most of the cross coefficients are negative. All the reported data was used to derive the ternary interaction mobility parameters.

4. Results and discussions

The thermodynamic factor of the diffusion coefficients can be readily derived from a CALPHAD-type thermodynamics database. The thermodynamic descriptions of the U–Zr, U–Pu and Pu–Zr

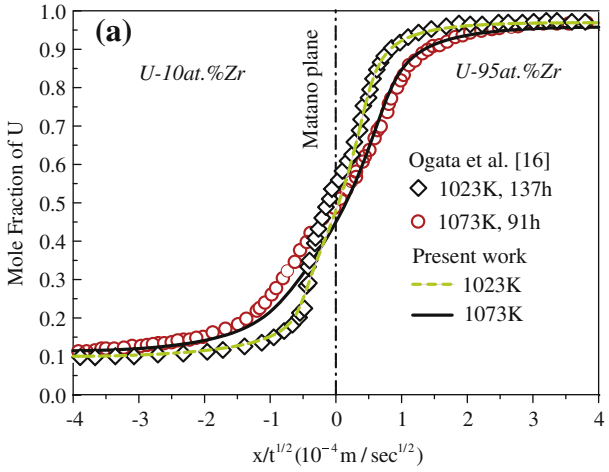

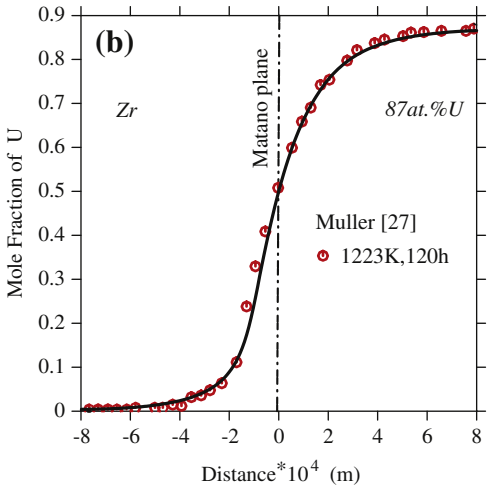

Fig. 5. Simulated concentration profiles of (a) the U-10 at.% Zr/U-95 at.% Zr binary couple at 1023 K and 1073 K and (b) the Zr/U-13 at.% Zr binary couple at 1223 K.

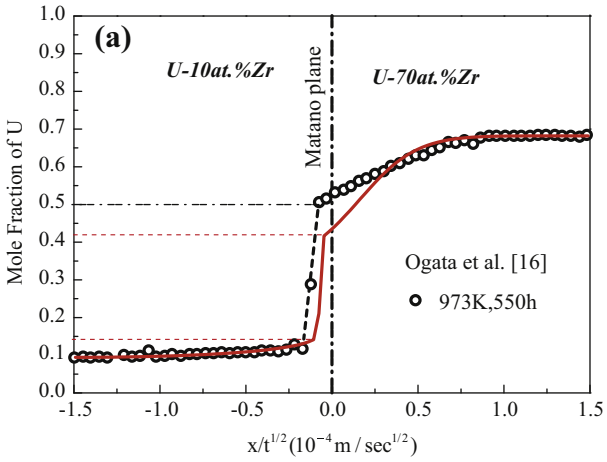

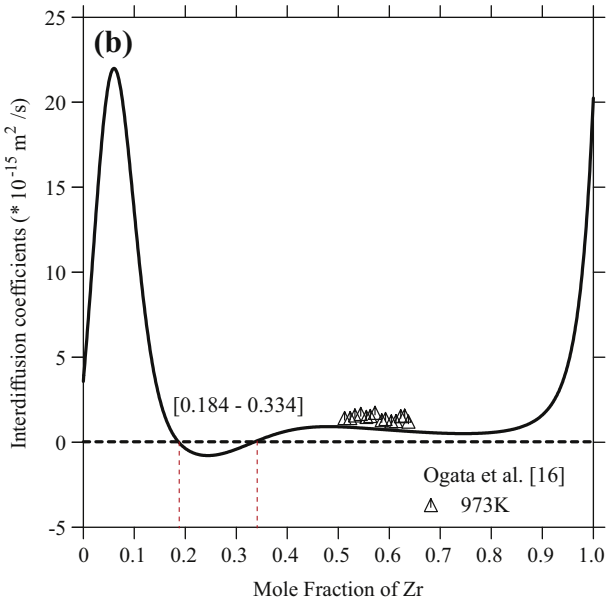

Fig. 6. (a) Calculated concentration profile for the U-10 at.% Zr/U-70 at.% Zr diffusion couple at 973 K for 550 h and (b) calculated interdiffusion coefficients in the U–Zr binary system at 973 K.

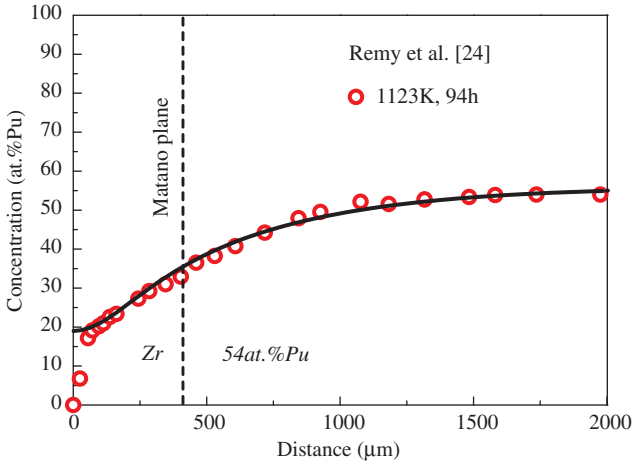

Fig. 7. Calculated concentration profile for the Zr/Zr-54 at.% Pu diffusion couple at 1123 K for 94 h. Symbols are from the experimental measurements [24].

binaries were taken from Chevalier et al. [25] and Kurata [1], respectively. The description of the U–Pu–Zr ternary system was extrapolated from the three sub-binaries since there is currently no assessed thermodynamic data for the ternary. The mobility of U in bcc-Zr was taken from the work of Fedorov et al. [15]. The mobility of the bcc-Zr self-diffusion has been previously assessed by using a piecewise polynomial [26]. However, in order to better represent its nonlinear Arrhenius relation while keep a clearer physical meaning, an expression, $D = D_1 \exp(-Q_1/RT) + D_2 \exp(-Q_2/RT)$, was used to reassess the mobility of self-diffusion in bcc-Zr in this work. All the other parameters were optimized by fitting the selected experimental tracer diffusivity and the interdiffusion coefficients by using the DICTRA software. The mobility parameters obtained in this work are given in Table 2.

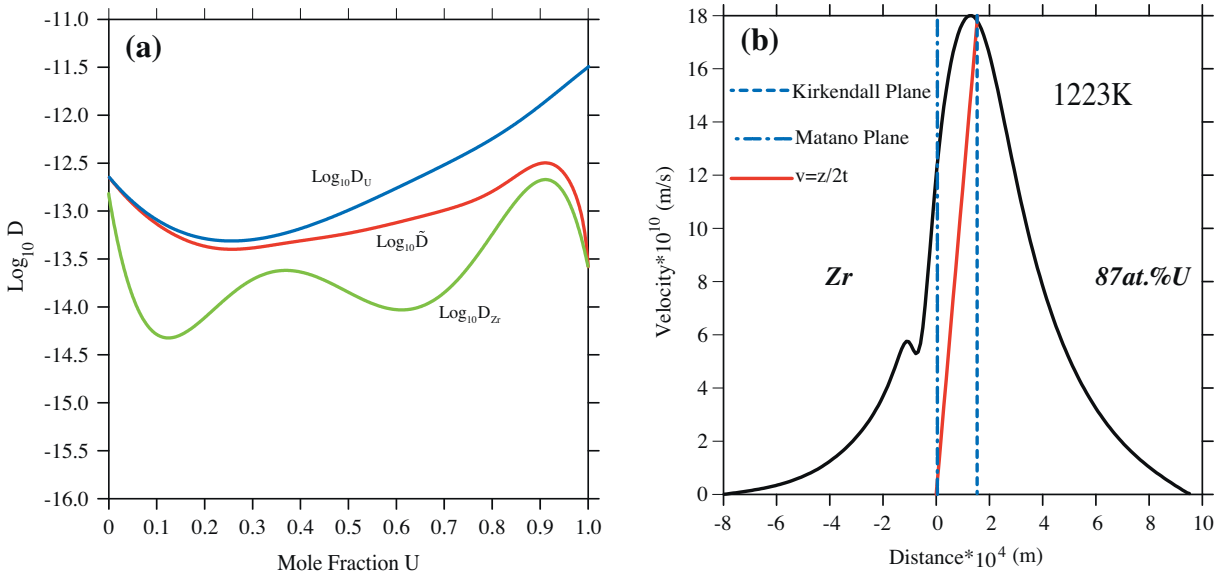

Fig. 8. (a) Intrinsic and interdiffusion coefficients in the U–Zr system at 1223 K; (b) Kirkendall velocity construction for the Zr/U-13 at.% Zr diffusion couple at 1223 K.

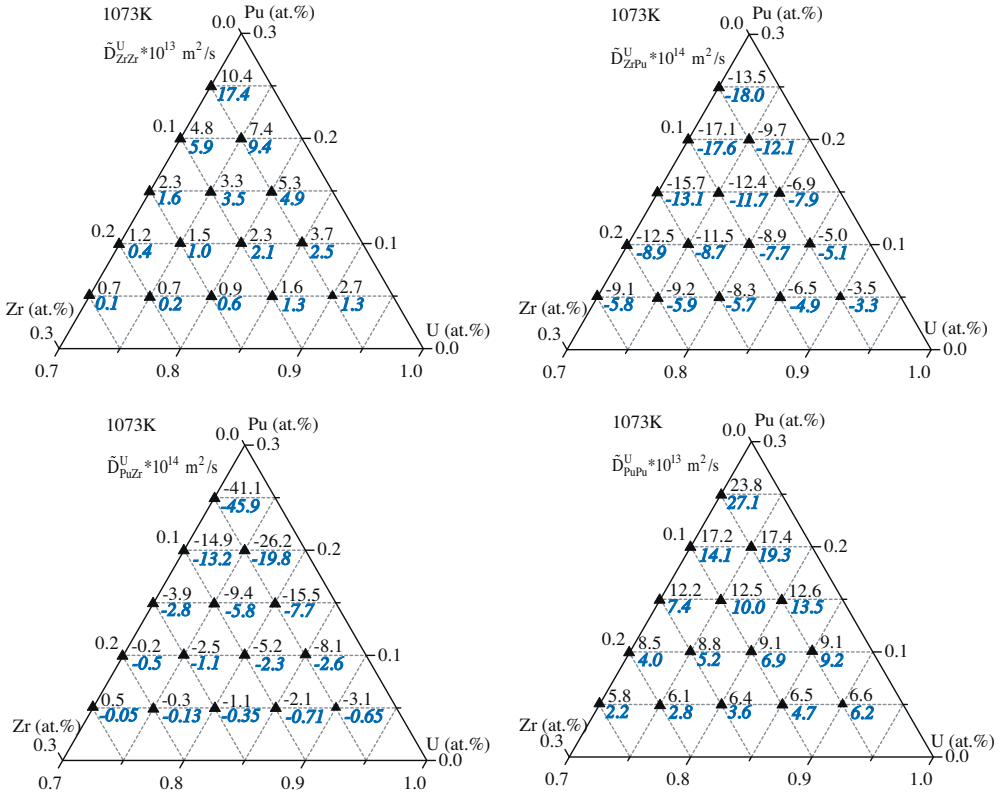

Fig. 9. Calculated interdiffusion coefficients (*italic numbers*) of the ternary U–Pu–Zr bcc alloys at 1073 K compared with the theoretical calculation [6].

4.1. U–Zr and Pu–Zr binaries

Validation of the assessed mobility parameters can be carried out by using them to calculate various diffusion coefficients. Fig. 2 shows that the calculated self and tracer diffusivities of the U–Zr binary alloys compare favorably with the experimental data [10–14]. Comparison for the interdiffusion coefficients is shown in Fig. 3 between the calculated and experimental points [16–19]. Note that the present calculation accurately represents the complex variation of the U–Zr interdiffusion coefficients in concentration. The agreement is less good at low temperatures, 1023 K and 1073 K, in Fig. 3a. This discrepancy might be because the two temperatures are close to the miscibility gap, as a result, short ordering begins to take effect and reduce the interdiffusion. Unfortunately, the short ordering effect has not been included in the DICTRA-type diffusion model. The discrepancy may also arise from the relatively large uncertainty in determination of the interdiffusion coefficients within or near a miscibility gap. Fig. 4 shows the very good agreement of the self, impurity and interdiffusion data in the Pu–Zr binary system.

Further validation can be made by comparing the predicted in-depth diffusion behavior resulting from interdiffusion with the measured data. In conjunction with the thermodynamics database, solving Eq. (6) numerically enables much of the diffusion-couple experiment to be predicted. Fig. 5a presents an example for the semi-infinite U-10 at.% Zr/U-95 at.% Zr diffusion couple annealed at 1023 K and 1073 K, respectively. Note that the simulated concentration profiles are in reasonable agreement with the measured points, [16] although the agreement is less good in the region close to the miscibility gap due to the reasons addressed before. By contrast, our predictions of the interdiffusion at the higher temperatures, not being affected by the miscibility gap, reproduce the measured data [27] very well, see Fig. 5b for the Zr/U-13 at.% Zr diffusion couple at 1223 K.

The prediction of the U-10 at.% Zr/U-70 at.% Zr couple at 973 K is shown in Fig. 6a. Note that the interdiffusion is strongly suppressed in and close to the miscibility gap. This can be further understood by the calculated interdiffusion coefficients at 973 K in Fig. 6b, which change a sign to negative between 18.4–33.4 at.% Zr, indicting that up-hill diffusion can occur. However, it is apparent that the calculated composition range is smaller than the observed values [16]. The reason for this might be twofold, one is the thermodynamic description of the U–Zr binary used in this work predicts a narrower miscibility gap; the other is that the high oxygen content in the starting materials of the diffusion couples [16] may expand the miscibility gap of the U–Zr system [29].

The predicted concentration profile is compared with the experimental data [24] in Fig. 7 for the Zr/Zr-54 at.% Pu diffusion couple. Note that the predicted Zr content was somewhat overestimated at the Zr-rich corner due to the fact that the diffusion couple was simplified as a bcc single-phase couple in the diffusion modeling. In reality the couple should have both the hcp and bcc phases at 1123 K and generally an hcp phase has a lower diffusion rate than a bcc phase.

As indicated by Eq. (7), the velocity of the inert markers can be determined from the knowledge of intrinsic diffusivities and the composition gradient at the marker position. Fig. 8a shows variations of two intrinsic diffusivities D_U and D_{Zr} and the interdiffusion coefficients in composition at 1223 K. It is apparent that the intrinsic diffusivity D_{Zr} is smaller than D_U over the whole concentration range, indicating that U is the fast diffuser if a diffusion couple is fabricated. Fig. 8b shows the Kirkendall velocity construction for the Zr/U-13 at.% Zr diffusion couple, indicating that the Kirkendall

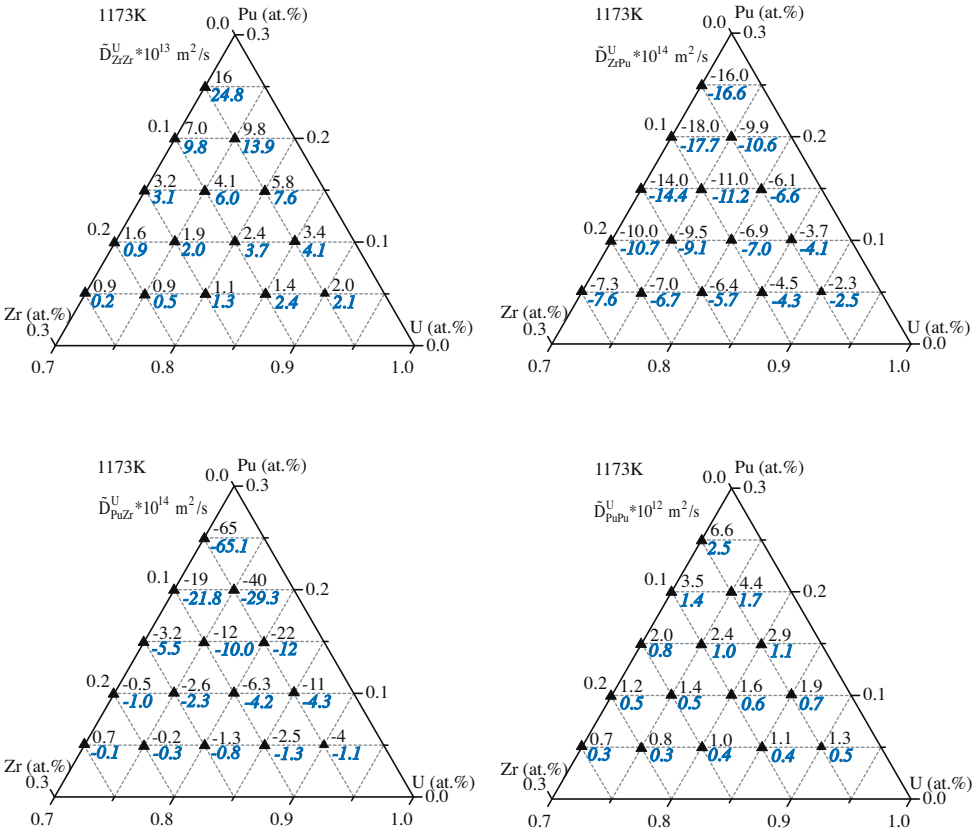

Fig. 10. Calculated interdiffusion coefficients (*italic numbers*) of the ternary U–Pu–Zr bcc alloys at 1173 K compared with the theoretical calculation [7].

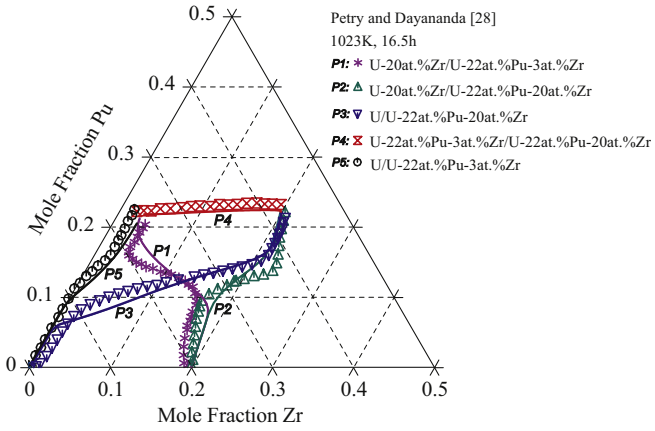

Fig. 11. Simulated diffusion paths for ternary couples compared with the experimental measurements (*symbols*) [28].

plane shifts toward the U-rich side and this is in accord with the finding of Muller [27].

4.2. U–Pu–Zr ternary

The calculated main and cross ternary interdiffusion coefficients are compared in Figs. 9 and 10 with the reported data from Alekseev et al. [6] at 1073 K and from Shmakov and Smirnov [7] at 1173 K, respectively. The agreements are satisfactory. As can be seen, two main coefficients $\tilde{D}^{U}_{PuPu}$ and $\tilde{D}^{U}_{ZrZr}$ strongly increase with increasing Pu and decreasing Zr, whereas the cross coefficients $\tilde{D}^{U}_{PuZr}$ and $\tilde{D}^{U}_{ZrPu}$ become more negative. Simulated diffusion paths, i.e. the curves on the ternary isotherm mapping the locus of the compositions in planes parallel to the couple interface throughout the diffusion zone, for the diffusion couples fabricated by Petry and Dayananda [28] are compared with the experimental points in Fig. 11. The agreement is fair for all the diffusion couples because there is no diffusion rate from Petry and Dayananda [28] and the diffusion path alone can not be directly used in the optimization process to further improve the present assessment.

5. Conclusion

The experimental diffusion data was evaluated to assess the atomic mobility for the bcc phase of the U–Zr and Pu–Zr binaries and the U–Pu–Zr ternary by using the DICTRA software. Good agreements were obtained from comprehensive comparisons made between the calculated diffusion coefficients and the available experimental values. The developed atomic mobility database, in conjunction with the CALPHAD-base thermodynamic description, has been successfully used to predict a large number of binary and ternary diffusion-couple experiments. The agreements are good for most of the diffusion couples annealed at higher temperatures, however, they are less good for the temperatures close to the miscibility gap. Most likely, this is caused by the up-hill diffusion and the short ordering effect.

Acknowledgements

This work was financially supported by the fund of the State Key Laboratory of Solidification Processing in Northwestern Polytechnical University, and the Program of Introducing Talents of Discipline in the Project of Advanced Materials and their Forming Technology (No. B08040).

Reference

[1] M. Kurata, Calphad 23 (1999) 305–337.
[2] Z.S. Li, X.J. Liu, C.P. Wang, J. Alloys Compd. 476 (2009) 193–198.
[3] D.R. Haeffner, J.B. Cohen, Acta Metall. Mater. 40 (1992) 831.
[4] J.O. Andersson, J. Ågren, J. Appl. Phys. 72 (1992) 1350–1355.
[5] T. Ogawa, T. Iwai, J. Less-Common Met. 170 (1991) 101–108.
[6] O.A. Alekseev, E.A. Smirnov, A.A. Shmakov, At. Energ. 84 (1998) 322–328.
[7] A.A. Shmakov, E.A. Smirnov, Defect Diffus. Forum 194–199 (2001) 229–234.
[8] B. Jonsson, Z. Metallkd. 85 (1994) 498–501.
[9] O. Redlich, A.T. Kister, Ind. Eng. Chem. 40 (1948) 345–348.
[10] Y. Adda, A. Kirianenko, J. Nucl. Mater. 2 (1959) 120–126.
[11] A. Bochvar, V. Kuznetsova, V. Sergeev, in: Transactions of the Second Geneva Conference on the Peaceful Uses of Atomic Energy, vol. 6, United Nations, Geneva, 1958, p. 68.
[12] R.V. Patil, J. Nucl. Mater. 187 (1992) 197–203.
[13] T.S. Lundy, J.I. Federer, R.E. Pawel, F.R. Winslow, in: J.A. Wheeler Jr., F.R. Winslow (Eds.), ASM, 1965 (Chapter 3).
[14] G.B. Fedorov, E.A. Smirnov, F.I. Zhomov, Metall. Phys. Metall. Pure Met. 7 (1968) 116–123.
[15] G.B. Fedorov, E.A. Smirnov, F.I. Zhomov, V.N. Gusev, S.A. Paraev, Atomnaya Énergiya 31 (1971) 516–518.
[16] T. Ogata, M. Akabori, A. Itoh, T. Ogawa, J. Nucl. Mater. 232 (1996) 125–130.
[17] L.V. Pavlinov, Atomnaya Énergiya 22 (1967) 290–292.
[18] Y. Adda, J. Philibert, Comptes Rendus de l Academie des Sciences Serie III: Sciences de la Vie 242 (1956) 3081–3086.
[19] Y.A. Shevchuk, At. Énerg. 82 (1997) 351–355.
[20] M. Akabori, A. Itoh, T. Ogawa, T. Ogata, J. Alloys Compd. 271–273 (1998) 597–601.
[21] M. Dupy, D. Calais, Trans. Metall. Soc. Aime 242 (1968) 1679–1684.
[22] Warren Z. Wade, David W. Short, John C. Walden, Joseph W. Magana, Metall. Trans. A 9A (1978) 965–972.
[23] J. Cornet, J. Phys. Chem. Solids 32 (1971) 1489.
[24] C. Remy, M. Dupuy, D. Calais, J. Nucl. Mater. 34 (1970) 46–58.
[25] P. Chevalier, E. Fischer, B. Cheynet, Calphad 28 (2004) 15–40.
[26] Y. Liu, L. Zhang, T. Pan, D. Yu, Y. Ge, Calphad 32 (2008) 455–461.
[27] N. Muller, Z. Metallk. 50 (1960) 652–660.
[28] M.C. Petry, M.A. Dayananda, J. Nucl. Mater. 240 (1997) 131–143.
[29] S.T Zegler, USAEC Rep. ANL-6055, 1962.